Exploring the phase partitioning in different cloud types using active and passive satellite sensors

Olimpia Bruno[1], Corinna Hoose[1], Trude Storelvmo[2], Quentin Coopman[1], Martin Stengel[3]

[1]Institute of Meteorology and Climate Research, Karlsruhe Institute of Technology, Karlsruhe, Germany
[2]Department of Geosciences, University of Oslo, Oslo, Norway
[3]Deutscher Wetterdienst (DWD), Offenbach am Main, Germany

Key Points:

- Despite fundamental differences and limitations, the retrievals based on a passive and an active satellite sensor agree with each other
- Supercooled liquid fraction is larger in the Southern Hemisphere than in the Northern Hemisphere, except for continental low-level clouds
- In clouds with temperatures between −40°C to 0°C, supercooled liquid fraction increases with optical thickness

Corresponding author: Olimpia Bruno, `olimpia.bruno@kit.edu`

Abstract

One of the largest uncertainties in numerical weather prediction and climate models is the representation of mixed-phase clouds, in which supercooled liquid water and ice can coexist. The aim of our study is to understand how the supercooled liquid fraction (SLF) in clouds with temperature from -40°C to 0°C is related to temperature, geographical location, and cloud type. Our analysis contains a comparison of four satellite-based datasets, one derived from active and three from passive satellite sensors, and focuses on SLF distribution near-globally, but also stratified by hemisphere and continental/maritime regions. Despite the SLF differences found among the datasets, they commonly indicate an increase of SLF with COT, and generally larger SLF in the Southern Hemisphere than in the Northern Hemisphere (up to about 20% difference), with the exception of continental low-level clouds, for which the opposite is true.

Plain Language Summary

In mixed-phase clouds, hydrometeors consisting of ice and supercooled liquid water, i.e. water below 0°C, can exist simultaneously. In the mixed-phase temperature range (-40°C to 0°C), ice-nucleating particles (e.g. mineral dusts, biological aerosol particles) are needed for glaciation to be possible. The partitioning into liquid and ice depends not only on the ice-nucleating particles, but also, for example, on cloud dynamics and ice multiplication processes, influencing in turn the lifetime and the precipitation type of these clouds, and the Earth-atmosphere energy balance locally and globally. In this study, we show ice and liquid partitioning for different cloud types, comparing four satellite-based datasets. This allows us to identify robustly their common trends despite their differences. Our results show on average less ice in the Northern than in the Southern Hemisphere when considering all clouds together, and that the larger the cloud optical thickness, the less ice when trating the cloud types separately. The partitioning of cloud types over sea and over land in both hemispheres show less ice in the Southern than in the Northern Hemisphere for high- and mid-level clouds, but the opposite for low-level clouds over land. This might be due to differences in aerosol composition and distribution.

1 Introduction

Mixed-phase clouds, i.e. clouds in which ice particles and supercooled liquid water can coexist in the temperature range of approximately -40°C to 0°C, are not fully understood yet and therefore not well represented in weather and climate models (McCoy et al., 2016).

Several studies have shown that mixed-phase clouds occur irrespective of the season, can be found in diverse locations, and can be associated with various cloud types (Korolev et al., 2017). Observations of mixed-phase clouds include satellite (i.e. Tan et al., 2014; Cesana & Storelvmo, 2017; Coopman et al., 2019), airborne in situ (i.e. Korolev, 2008; Costa et al., 2017; Barrett et al., 2020), ground-based (i.e. Henneberger et al., 2013; Gierens et al., 2019) and aircraft-based remote sensing measurements (i.e. Wang et al., 2012; Plummer et al., 2014). In Tan et al. (2014), in particular, mixed-phase clouds have been studied statistically in terms of supercooled cloud fraction (SCF), defined as the ratio of the in-cloud frequency of supercooled liquid pixels to the total frequency of supercooled liquid and ice pixels within 2° latitude by 5° longitude grid boxes, at several isotherms between -10°C and -30°C, distinguishing cases in the Northern Hemisphere (NH) and in the Southern Hemisphere (SH), as well as cases over ocean and over land. This study consisted of the analysis of about five years of data from NASA's spaceborne lidar, CALIOP (Cloud-Aerosol Lidar with Orthogonal Polarization) level 2 Vertical Feature Mask (VFM) in versions 3.01 and 3.02, and the relationship between cloud phase and several aerosol types was determined. They found that dust aerosols might strongly influence the SCF by acting as ice-nucleating particles (INPs), illustrating how important the atmospheric aerosol composition can be for the cloud phase. Moreover, larger SCF in the SH than in the NH has been found, which may be caused by the presence of more land in the NH, where efficient INPs originate. This result may also explain why larger SCF has been found over land than over ocean.

As in Tan et al. (2014), we apply a similar statistical approach to quantify the phase distribution of mixed-phase clouds on isotherms. In addition, we reproduce the International Satellite Cloud Climatology Project (ISCCP) cloud classification (Rossow & Schiffer, 1999) to distinguish different cloud types. Our study includes data from passive (Advanced Very High Resolution Radiometer — AVHRR) and active (Cloud-Aerosol Lidar and Infrared Pathfinder Satellite Observation — CALIPSO) satellite sensors, with the intention to identify robust signals despite differences, facilitating the potential identification of common features based on different sources and algorithms. Passive sensors offer the benefit of long-period records with daily near-global coverage, which motivates us to compare three AVHRR-based datasets with the CALIPSO-based dataset, and to present this work as a validation study.

After a description of the datasets and the method in Section 2, Section 3 contains the analysis and the results of our study, while conclusive discussions are presented in Section 4.

2 Datasets and Method

2.1 Datasets

The datasets we analyzed are Cloud_cci AVHRR-PMv2 (Stengel et al., 2017), Cloud_cci AVHRR-PMv3 (Stengel et al., 2020), CLARA-A2 (Karlsson et al., 2017), and CALIOP level 2 Cloud Layer Data in version 4.20 (Z. Liu et al., 2019). While the first three are based on the polar-orbiting passive satellite sensor AVHRR (only a NOAA-19 subset is used here), CALIOP is an active sensor onboard the polar-orbiting CALIPSO satellite.

The AVHRR datasets provide cloud top information as global composites with a spatial resolution of 0.05°x0.05°, containing data twice per day from ascending and descending for each location. The swath width of AVHRR is wide enough to provide global coverage daily. The AVHRR sensor has five to six channels located in the near-infrared (NIR), the infrared (IR), and the visible (VIS) ranges. The measurements are used to perform cloud detection and to retrieve cloud top phase, cloud top pressure, cloud optical thickness, and cloud particle effective radius. From these variables cloud top temperature, cloud top height, cloud liquid/ice water path are produced. For retrieving the cloud top phase, Cloud_cci v2 and CLARA-A2 use a threshold scheme (Pavolonis & Heidinger, 2004; Pavolonis et al., 2005), while Cloud_cci v3 uses a neural network trained with CALIOP v3. The provided cloud top phase consists of a binary flag (liquid/ice); no mixed-phase case is given. AVHRR-based retrievals often lack sensitivity to high, optically very thin cloud layers, which might be missed or associated with larger uncertainties in the retrieved cloud properties (Stengel et al., 2015).

Part of the NASA A-Train, CALIOP provides vertical distributions of clouds and aerosols along so-called “granules”. A granule is an orbit segment containing cloud, temporal, and geographical information for every vertical profile. The spatial resolution of CALIPSO is 333 m, while the vertical resolution is 30-60m. In our analysis we use CALIOP level 2 Cloud Layer Data in version 4.20 with a spatial resolution of 5 km, corresponding to approximately 0.05° as in AVHRR at the equator. The swath width is very narrow, so that about one month of data must be collected to obtain a near-global coverage. The cloud altitude is derived as primary product, which is also converted to temperatures using model data from Goddard Earth Observing System, Version 5 (GEOS-5) vertical profiles. The cloud phase is retrieved using the depolarization of backscattered light, distinguishing liquid water from “randomly-oriented” and “horizontally-oriented” ice ("ROI" and "HOI", respectively). The dataset provides vertical distributions of clouds in layers. Every layer can contain only one thermodynamic phase. CALIOP is able to retrieve up to an optical thickness of approximately 5 into the cloud (Karlsson & Håkansson, 2018).

2.2 Method

We analyzed near-global (60° N to 60° S) data from 1 June 2009 to 31 May 2013. As the cloud optical thickness, involved in the cloud type classification, can be detected by the AVHRR sensor only by the channels in the visible range, we consider only daytime measurements, i.e. the ascending track; we do the same for CALIOP to make the comparison as consistent as possible, although daytime CALIOP retrieval has a higher backscatter sensitivity threshold (Winker et al., 2009). We constrain further analyses for latitudinal bands as follows: NH – from 60° N to 30° N; SH – from 30° S to 60° S. Continental and maritime regions are analyzed separately. Because from AVHRR only the cloud top information is available, we investigate the cloud top phase distribution in relation to the cloud top temperature, with a focus on the mixed-phase temperature range. With a four-year analysis, we provide statistics on the supercooled liquid fraction (SLF) in clouds. The SLF is computed as the ratio between the number of liquid cloud top pixels and the sum of ice plus liquid cloud top pixels in a given temperature interval. The analyzed isotherms cover the range -60°C to 5°C, with a 1°C increment. To sort the cloud types, the ISCCP classification (Rossow & Schiffer, 1999) is used, based on threshold values of cloud top pressure (CTP) and cloud optical thickness (COT). Considering the differences between the sensors, a filter for COT is applied to make the detected clouds as comparable as possible. For AVHRR datasets, all the cloudy pixels with COT < 0.3 are filtered out. To be comparable to AVHRR datasets and mimic the view of the passive sensor, we remove the uppermost layers from the CALIOP profiles down to an optical thickness of 0.3 and consider the remaining highest cloud top layer for the study. The cloud classification precedes the computation of SLF on isotherms in the studies in which different cloud types are analyzed.

3 Results

Figure 1 shows the relationships between cloud top temperature (CTT) and SLF for all datasets for the entire area of interest (a), comparing the extratropical Northern and Southern Hemispheres (b), as well as land and ocean (c), and considering only continental pixels (d) and maritime pixels (e) for Northern vs Southern Hemispheres. The difference in SLF and the associated CTT among the datasets stands out in these figures, and in particular the gap between the three AVHRR-based datasets and CALIOP, up to about 20°C or SLF of about 80% at a fixed temperature.

There are many possible reasons for these differences. One of the most important ones is the small impact of optically thin clouds on the radiation measured by AVHRR, potentially leading to large errors in cloud retrievals for these cloud layers. In fact, a separation of the near-global plot into different cloud types (not shown) shows that, for the optically thickest clouds (e.g., stratus, nimbostratus, and deep convective clouds) detected by AVHRR, the increase of SLF with CTT is more similar to CALIOP. But looking at the frequency of occurrence of different cloud types on isotherms (not shown), the optically thickest clouds detected by AVHRR are far fewer than clouds with COT < 23, and contribute less to the near-global result shown in Fig. 1(a). Another reason which may contribute to this difference is dependent on the sensors, the first passive and the second active. Furthermore, the filter we applied to the optical thickness may be not sufficient to make sure that we are analyzing the cloud data in the same way: While the AVHRR has problems detecting multilayer clouds that include top layers with small COT, leading to misclassifications of cloud top phase, CALIOP can detect multilayer clouds

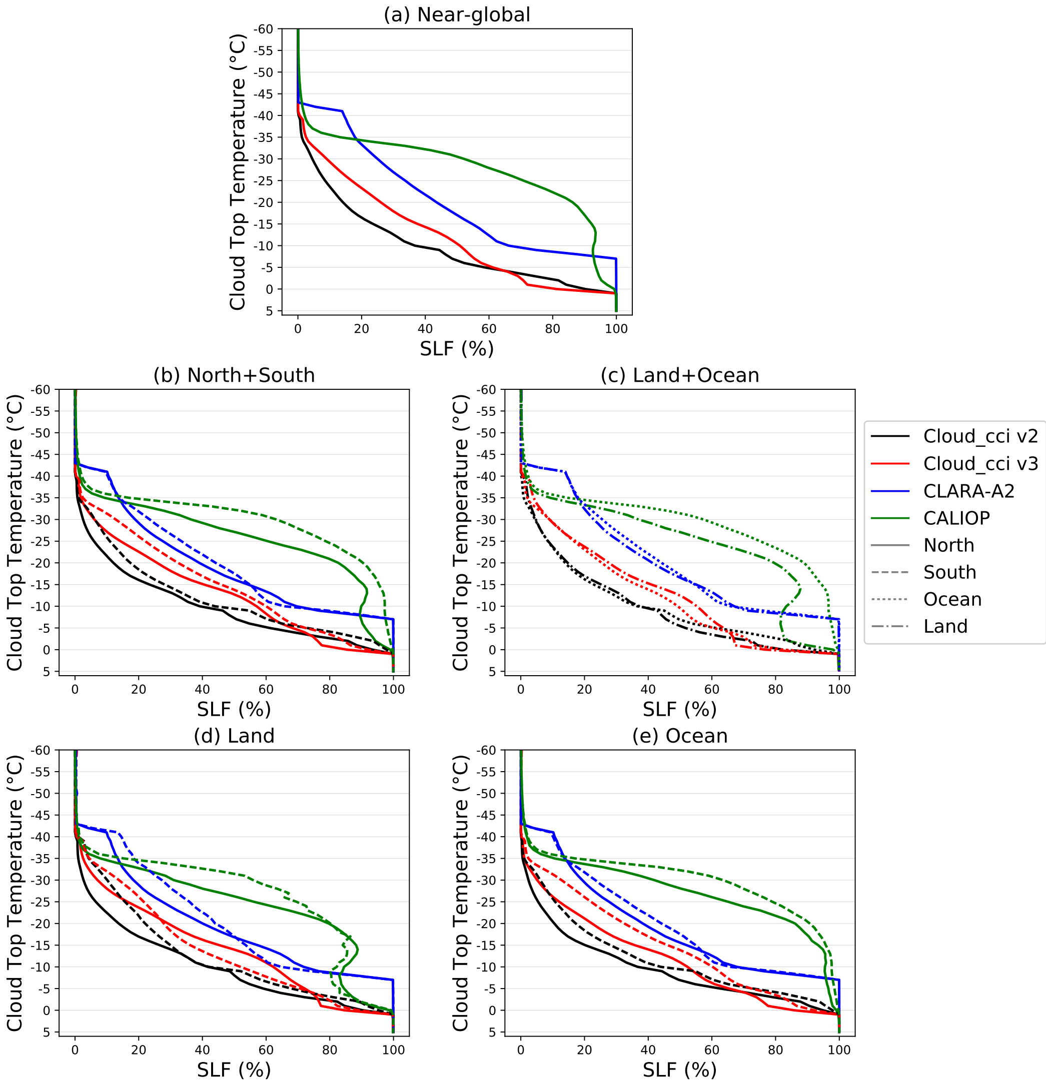

Figure 1. Comparison of supercooled liquid fractions (SLFs) considered (a) near-globally, (b) over the extratropical Northern and the Southern Hemispheres, (c) over land and ocean, (d) over only continental pixels over extratropical Northern and Southern Hemispheres, and (e) over only maritime pixels over extratropical Northern and Southern Hemispheres. Different colors represent different datasets; different line types represent different areas of interest.

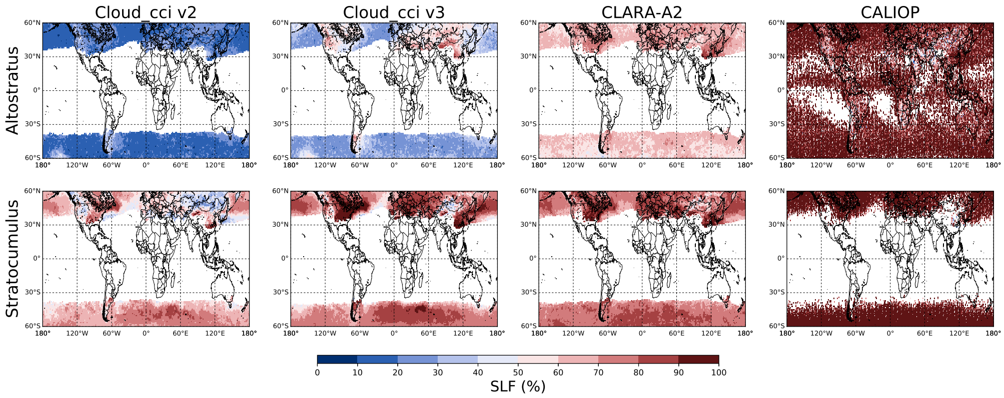

Figure 2. Geographical distribution of the supercooled liquid fraction (SLF) for altostratus (top) and stratocumulus (bottom) clouds in the analyzed datasets at the isotherm T $= (-10 \pm 2.5)°$C.

with optical thickness up to 5, and this might cause misclassifications too. Moreover, a possible phase change of a detected cloud top would cause a modification of COT, and therefore a possible misclassification to an optically thicker or thinner cloud category, modifying the SLF of another cloud type. Some of these issues have also been presented in Cesana et al. (2019) for shallow cumulus and stratocumulus clouds, emphasizing that errors in retrieving cloud phase, cloud optical thickness, and cloud top height can result in cloud type misclassifications. A quantitative analysis of the differences between CALIOP and Cloud_cci v2 and v3 can be found in Stengel et al. (2020): While any phase bias of Cloud_cci v2 and v3 with respect to CALIOP has nearly vanished for COTs of approximately 0.15 into the clouds, there is still a significant bias at COT = 1 for the cloud top height of ice clouds, to which CTT is linked. As a consequence, the too-warm ice clouds retrieved by AVHRR retrievals likely bias the SLF low for probably all CTT, agreeing to our results. In Stengel et al. (2015), CALIOP's liquid cloud fraction resulted closer to the AVHRR-based dataset CLAVR-x (Cloud from AVHRR Extended) than to other AVHRR-based datasets. One reason was that for CLAVR-x algorithms a priori information based on CALIOP climatologies was used for ice clouds. This in turn prevented that phase and CTT were independently retrieved, condition required for our study.

Figure 2 shows the geographical distribution of SLF for two cloud types (altostratus and stratocumulus) at the isotherm T $= (-10 \pm 2.5)°$C for the different datasets. For each geographical distribution, only the pixels with a frequency of occurrence greater than 2% with respect to the maximum frequency of occurrence have been plotted. The disagreements the datasets exhibit could be due to shortcomings in the passive imager CTT retrievals. At that temperature, CALIOP retrieves many more liquid cloud tops than the AVHRR-based datasets, and not only for low-level clouds like stratocumulus, but also for the altostratus clouds, occurring also in the Tropics, mainly over continents, and over the Intertropical Convergence Zone. Moreover, this may also be an indicator of cloud type misclassification linked to the retrieved cloud phase and optical thickness. AVHRR-based datasets show differences in SLF too: The maritime altostratus clouds show more ice content in Cloud_cci v2 and v3 than in CLARA-A2, whereas SLF $> 50\%$ over continents for Cloud_cci v3 as well as for CLARA-A2, but not for Cloud_cci v2. Tthis figure shows also how SLF over ocean or over land can considerably change for a single isotherm when considering cloud at different height levels, and therefore how different aerosols can influence the cloud phase depending on cloud height, location, and temperature (Villanueva et al., 2020).

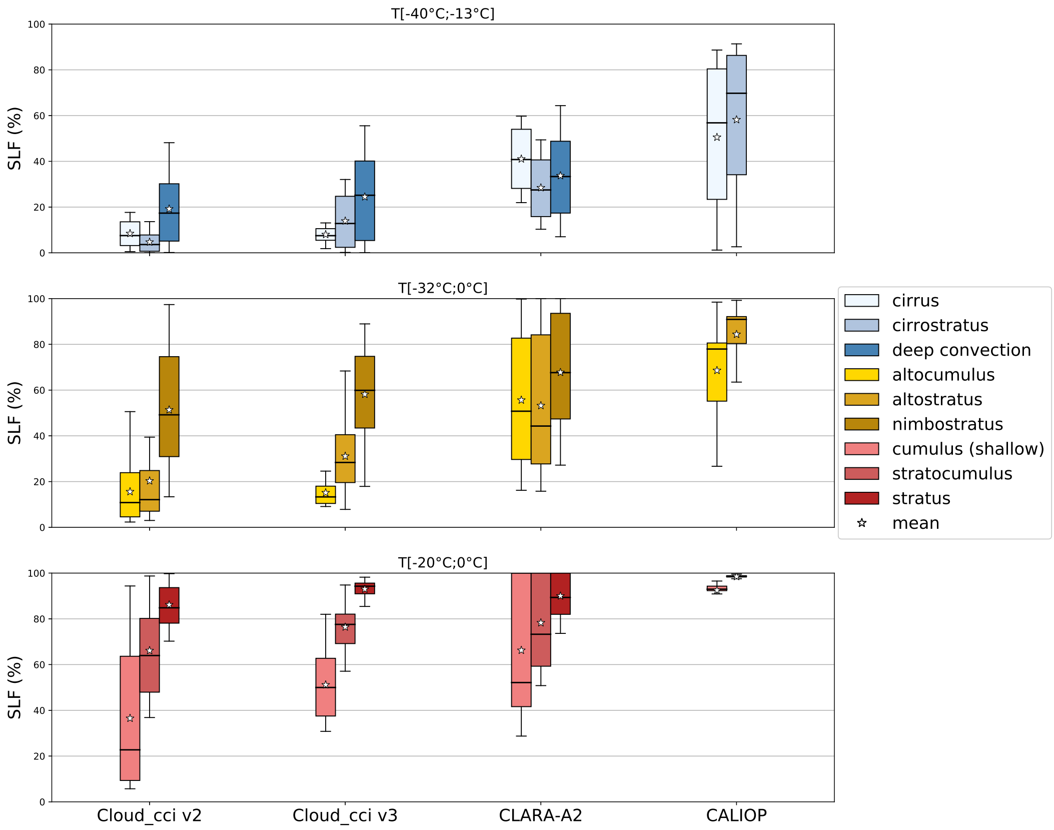

Figure 3. Boxplot of the supercooled liquid fraction (SLF) for different cloud types collected in three height levels. Clouds in the same level share the same temperature range. The different datasets are separated by columns and every color corresponds to one cloud type. The boxes extend from the lower to upper quartile values of the data, whereas the whiskers show the entire range of the data. The horizontal lines within the boxes represent the median of the distributions, while the stars represent their mean values.

Despite the differences, the datasets also exhibit consistencies. For a given temperature, SLF tends to be higher in the SH than in the NH (Fig. 1(b)), and this is valid for all considered datasets: This result is in line with Tan et al. (2014). There is no agreement among the datasets considering SLF over land and ocean (Fig. 1(c)), where only CALIOP shows clearly higher SLF over ocean than over land, again consistent with Tan et al. (2014). The pattern of higher SLF in the NH than in the SH is more evident when constraining the analysis to maritime pixels only (Fig. 1(e)), while it's not confirmed by all datasets over land (Fig. 1(d)).

Figures 3 shows the global SLF distribution for different cloud types. The cloud types have been grouped into high-, mid-, and low-level clouds taking into account the temperature range that the datasets have in common in the three height categories respectively. In this figure, only the temperatures with frequency of occurrence greater than 2% with respect to the maximum of the distributions of every cloud type have been considered (anyway the sensitivity to this percentage considered as threshold is low). Similarly to Fig. 1, in Fig. 3 the systematically lower SLF in AVHRR compared to CALIOP is found. Moreover, a further outcome can be identified in this figure for most cases: the optically thicker the clouds, the larger the SLF. This is true for every height level and almost all cases, and consistent in all datasets.

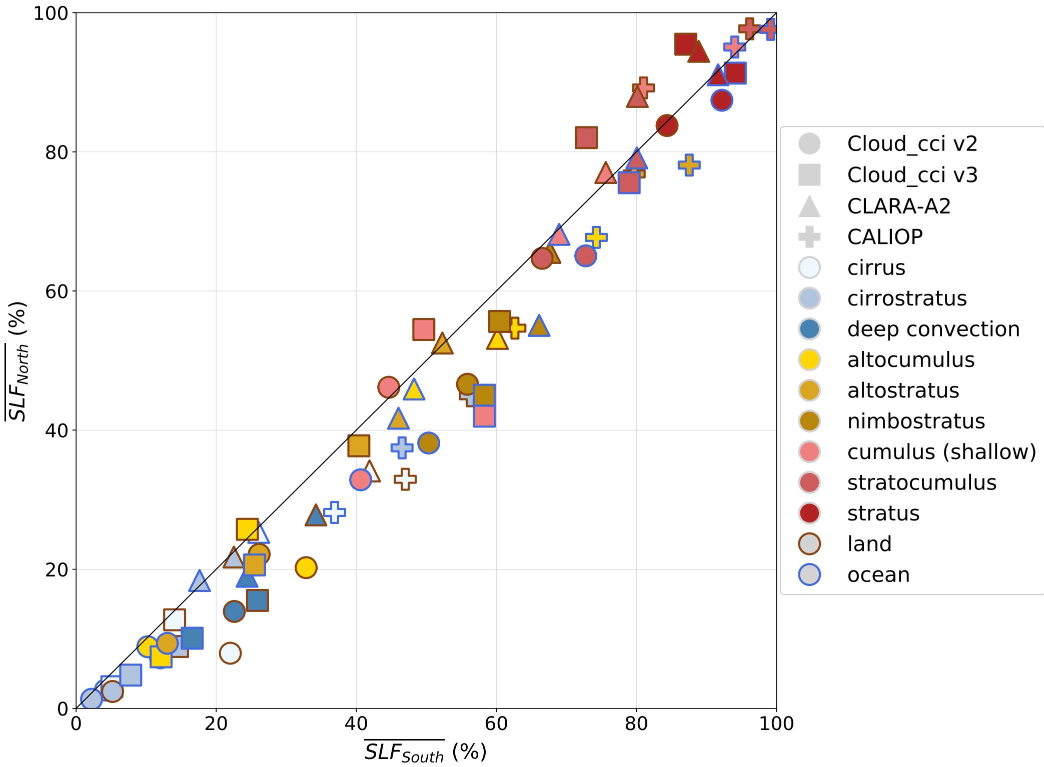

Figure 4. Comparison of mean supercooled liquid fraction (SLF) over extratropical Northern and Southern Hemisphere for different cloud types, considered in the temperature ranges they have in common for the same height. Different markers identify different datasets, filling colors distinguish the cloud types, while edge colors refer to continental or maritime pixels.

Figure 4 shows the mean SLF for the different cloud types and datasets, constraining the analysis for NH and SH, over ocean and over land. It gives the same results found in Figure 3, with larger SLF for optically thicker clouds. Furthermore, SLF is generally higher in the SH, with the exception of most low-level clouds over land (shallow cumulus, stratocumulus, and stratus clouds), for which SLF is higher in the NH.

4 Discussion and Conclusions

We performed a statistical analysis to better understand the relationship between cloud phase and temperature in the mixed-phase temperature range. Our study is based on four datasets (Cloud_cci AVHRR-PM2.0, Cloud_cci AVHRR-PM3.0, CLARA-A2, and CALIOP v4.20) and consists of the comparison of the retrieved cloud top phase and cloud top temperature in terms of SLF for specific isotherms. The analysis was conducted from 60° N to 60° S, for extratropical Northern and Southern Hemispheres separately, for continental and oceanic surfaces, and for different cloud types. To classify the cloud types, cloud top pressure and cloud optical thickness thresholds have been used (Rossow & Schiffer, 1999).

Despite the differences between active and passive retrievals for cloud top temperature and thermodynamic phase, which may also because of uncertainties in the cloud type classification, we found consistent results for all datasets. Summarizing the main findings:

- We found higher SLF in the SH than in the NH, in agreement with Tan et al. (2014). This result might be explained by the larger size of continental area and therefore the prevalence of continental aerosol with the ability to act as INPs in the NH. Higher SLF in the SH than in the NH was found also when constraining the analysis for maritime surfaces, while over-land cases did not show a common trend. In this paper, we showed that further analyses using different cloud types are necessary to better explain the global results.
- To explain the over-land result, we analyzed different cloud types in NH and SH, over land and over ocean. We found, also for different cloud types, larger SLF in the SH than in the NH, with the exception of the most low-level clouds over land, for which the opposite occurs. This might be due to the presence of drier conditions and thus more dust aerosols acting as INPs in the SH than in the NH. Considering that the common temperature range of the analyzed continental low-level clouds goes from $-14°$C to $0°$C, our result shows agreements with Villanueva et al. (2020), where lower ice content was found in clouds in NH than in SH for T $= -15° \pm 6°$C, probably because of the larger amount of feldspar in the SH. Moreover, our result could also be explained by the higher density of particles acting as CCN in the NH, resulting in smaller droplet sizes, which might limit secondary ice formation (Mossop, 1980). Further previous studies show agreements with our results: Some anthropogenic aerosols such as black carbon, sulfate, and organic aerosols, do not act as efficient INPs but are efficient CCNs (Hoose & Möhler, 2012); model outputs have shown that sulfate aerosol and black carbon have the highest mass concentration in the lower troposphere of the NH (X. Liu et al., 2009), where they act as CCN (Boucher & Lohmann, 1995), whereas they act as INPs only at very high altitudes over the Tropics and the polar regions (X. Liu et al., 2009). Indeed, Tan et al. (2014) found that dust (as mineral desert dust), polluted dust (as dust mixed with urban pollution and biomass burning smoke), and smoke (as biomass burning aerosols, principally made of soot and organic carbon) are mainly distributed in the Tropics and in the NH.
- In the analysis of different cloud types, same-height clouds show SLF increasing with COT. Two explanations are possible for this finding. On one hand, clouds containing more droplets than ice particles result in higher optical thickness. On

the other hand, optically thicker clouds tend to have stronger updrafts and consequently higher supersaturation values, which may inhibit the glaciation process (Korolev, 2007), potentially lowering the glaciation temperature in clouds and causing the presence of more supercooled liquid water than ice. From our analysis it is not possible to determine if one of the two described processes can univocally explain the obtained result.

In our analysis we have tried to take into account the possible limitations in the datasets mainly linked to the phase detection of the sensors. Because of this, particular attention has been paid to the cloud optical thickness, taking into account that the cloud top phase as well as cloud type might be influenced by it. Despite the differences found in the datasets, our results show broad agreements among them in many aspects, not only proving the robustness of the results but also showing that the passive satellite sensor AVHRR can contribute to the cloud phase research once its limitations have been taken into account. The AVHRR-based datasets can be used for further studies, benefiting from the long temporal record and good spatial coverage. A comparison with climate models is ongoing.

Acknowledgments

We acknowledge the usage of the datasets obtained from CM SAF (https://wui.cmsaf.eu), ESA Cloud_cci (http://www.esa-cloud-cci.org), and NASA Langley Research Center Atmospheric Science Data Center (https://eosweb.larc.nasa.gov/). This project has received funding from the European Research Council (ERC) under the European Union‘s Horizon 2020 research and innovation programme under grant agreement No 714062 (ERC Starting Grant “C2Phase”). This work was performed on the supercomputer ForHLR funded by the Ministry of Science, Research and the Arts Baden-Württemberg and by the Federal Ministry of Education and Research. We thank Jan Cermak for the helpful discussions.

References

Barrett, P. A., Blyth, A., Brown, P. R. A., & Abel, S. J. (2020). The structure of turbulence and mixed-phase cloud microphysics in a highly supercooled altocumulus cloud. *Atmospheric Chemistry and Physics*, *20*(4), 1921–1939. doi: 10.5194/acp-20-1921-2020

Boucher, O., & Lohmann, U. (1995). The sulfate-CCN-cloud albedo effect. *Tellus B: Chemical and Physical Meteorology*, *47*(3), 281–300. doi: 10.3402/tellusb.v47i3.16048

Cesana, G., Del Genio, A. D., & Chepfer, H. (2019). The Cumulus And Stratocumulus CloudSat-CALIPSO Dataset (CASCCAD). *Earth System Science Data Discussions*, *11*, 1–33. doi: 10.5194/essd-2019-73

Cesana, G., & Storelvmo, T. (2017). Improving climate projections by understanding how cloud phase affects radiation. *Journal of Geophysical Research*, *122*(8), 4594–4599. doi: 10.1002/2017JD026927

Coopman, Q., Hoose, C., & Stengel, M. (2019). Detection of Mixed-Phase Convective Clouds by a Binary Phase Information From the Passive Geostationary Instrument SEVIRI. *Journal of Geophysical Research: Atmospheres*, *124*(9), 5045–5057. doi: 10.1029/2018JD029772

Costa, A., Meyer, J., Afchine, A., Luebke, A., Günther, G., Dorsey, J. R., … Krämer, M. (2017). Classification of Arctic, midlatitude and tropical clouds in the mixed-phase temperature regime. *Atmospheric Chemistry and Physics*, *17*(19), 12219–12238. doi: 10.5194/acp-17-12219-2017

Gierens, R., Kneifel, S., Shupe, M., Ebell, K., Maturilli, M., & Löhnert, U. (2019). Low-level mixed-phase clouds in a complex Arctic environment. *Atmospheric*

Chemistry and Physics Discussions(July), 1–37. doi: 10.5194/acp-2019-610

Henneberger, J., Fugal, J. P., Stetzer, O., & Lohmann, U. (2013). HOLIMO II: A digital holographic instrument for ground-based in situ observations of microphysical properties of mixed-phase clouds. *Atmospheric Measurement Techniques*, *6*(11), 2975–2987. doi: 10.5194/amt-6-2975-2013

Hoose, C., & Möhler, O. (2012). Heterogeneous ice nucleation on atmospheric aerosols: A review of results from laboratory experiments. *Atmospheric Chemistry and Physics*, *12*(20), 9817–9854. doi: 10.5194/acp-12-9817-2012

Karlsson, K. G., Anttila, K., Trentmann, J., Stengel, M., Fokke Meirink, J., Devasthale, A., ... Hollmann, R. (2017). CLARA-A2: The second edition of the CM SAF cloud and radiation data record from 34 years of global AVHRR data. *Atmospheric Chemistry and Physics*, *17*(9), 5809–5828. doi: 10.5194/acp-17-5809-2017

Karlsson, K.-G., & Håkansson, N. (2018). Characterization of avhrr global cloud detection sensitivity based on calipso-caliop cloud optical thickness information: demonstration of results based on the cm saf clara-a2 climate data record. *Atmospheric Measurement Techniques*, *11*(1), 633–649. doi: 10.5194/amt-11-633-2018

Korolev, A. V. (2007). Limitations of the Wegener–Bergeron–Findeisen Mechanism in the Evolution of Mixed-Phase Clouds. *Journal of the Atmospheric Sciences*, *64*(9), 3372–3375. doi: 10.1175/JAS4035.1

Korolev, A. V. (2008). Rates of phase transformations in mixed-phase clouds. *Quarterly Journal of the Royal Meteorological Society*, *134*(632), 595–608. doi: 10.1002/qj.230

Korolev, A. V., McFarquhar, G., Field, P. R., Franklin, C., Lawson, P., Wang, Z., ... Wendisch, M. (2017). Mixed-Phase Clouds: Progress and Challenges. *Meteorological Monographs*, *58*. doi: 10.1175/AMSMONOGRAPHS-D-17-0001.1

Liu, X., Penner, J. E., & Wang, M. (2009). Influence of anthropogenic sulfate and black carbon on upper tropospheric clouds in the NCAR CAM3 model coupled to the IMPACT global aerosol model. *Journal of Geophysical Research: Atmospheres*, *114*(D3). doi: 10.1029/2008JD010492

Liu, Z., Kar, J., Zeng, S., Tackett, J., Vaughan, M., Avery, M., ... Winker, D. (2019). Discriminating between clouds and aerosols in the CALIOP version 4.1 data products. *Atmospheric Measurement Techniques*, *12*(1), 703–734. doi: 10.5194/amt-12-703-2019

McCoy, D. T., Tan, I., Hartmann, D. L., Zelinka, M. D., & Storelvmo, T. (2016, jun). On the relationships among cloud cover, mixed-phase partitioning, and planetary albedo in GCMs. *Journal of Advances in Modeling Earth Systems*, *8*(2), 650–668. doi: 10.1002/2015MS000589

Mossop, S. C. (1980). The mechanism of ice splinter production during riming. *Geophysical Research Letters*, *7*(2), 167-169. doi: 10.1029/GL007i002p00167

Pavolonis, M. J., & Heidinger, A. K. (2004). Daytime Cloud Overlap Detection from AVHRR and VIIRS. *Journal of Applied Meteorology*, *43*, 762–778. doi: 10.1175/2099.1

Pavolonis, M. J., Heidinger, A. K., & Uttal, T. (2005). Daytime Global Cloud Typing from AVHRR and VIIRS: Algorithm Description, Validation, and Comparisons. *Journal of Applied Meteorology*, *44*(6), 804–826. doi: 10.1175/JAM2236.1

Plummer, D. M., Mcfarquhar, G. M., Rauber, R. M., Jewett, B. F., & Leon, D. C. (2014). Structure and statistical analysis of the microphysical properties of generating cells in the comma head region of continental winter cyclones. *Journal of the Atmospheric Sciences*, *71*(11), 4181–4203. doi: 10.1175/JAS-D-14-0100.1

Rossow, W. B., & Schiffer, R. A. (1999). Advances in Understanding Clouds from ISCCP. *Bulletin of the American Meteorological Society*, *80*(11), 2261–2287.

doi: 10.1175/1520-0477(1999)080⟨2261:AIUCFI⟩2.0.CO;2

Stengel, M., Mieruch, S., Jerg, M., Karlsson, K. G., Scheirer, R., Maddux, B., ... Hollmann, R. (2015). The Clouds Climate Change Initiative: Assessment of state-of-the-art cloud property retrieval schemes applied to AVHRR heritage measurements. *Remote Sensing of Environment*, *162*, 363–379. doi: 10.1016/j.rse.2013.10.035

Stengel, M., Stapelberg, S., Sus, O., Finkensieper, S., Würzler, B., Philipp, D., ... McGarragh, G. (2020). Cloud_cci advanced very high resolution radiometer post meridiem (avhrr-pm) dataset version 3: 35-year climatology of global cloud and radiation properties. *Earth System Science Data*, *12*(1), 41–60. doi: 10.5194/essd-12-41-2020

Stengel, M., Stapelberg, S., Sus, O., Schlundt, C., Poulsen, C., Thomas, G., ... Hollmann, R. (2017). Cloud property datasets retrieved from AVHRR, MODIS, AATSR and MERIS in the framework of the Cloud-cci project. *Earth System Science Data*, *9*(2), 881–904. doi: 10.5194/essd-9-881-2017

Tan, I., Storelvmo, T., & Choi, Y. S. (2014). Spaceborne lidar observations of the ice-nucleating potential of dust, polluted dust, and smoke aerosols in mixed-phase clouds. *Journal of Geophysical Research*, *119*(11), 6653–6665. doi: 10.1002/2013JD021333

Villanueva, D., Heinold, B., Seifert, P., Deneke, H., Radenz, M., & Tegen, I. (2020). The day-to-day co-variability between mineral dust and cloud glaciation: a proxy for heterogeneous freezing. *Atmospheric Chemistry and Physics*, *20*(4), 2177–2199. doi: 10.5194/acp-20-2177-2020

Wang, Z., French, J., Vali, G., Wechsler, P., Haimov, S., Rodi, A., ... Pazmany, A. L. (2012). Single aircraft integration of remote sensing and in situ sampling for the study of cloud microphysics and dynamics. *Bulletin of the American Meteorological Society*, *93*(5), 653–668. doi: 10.1175/BAMS-D-11-00044.1

Winker, D. M., Vaughan, M. A., Omar, A., Hu, Y., Powell, K. A., Liu, Z., ... Young, S. A. (2009). Overview of the CALIPSO mission and CALIOP data processing algorithms. *Journal of Atmospheric and Oceanic Technology*, *26*(11), 2310–2323. doi: 10.1175/2009JTECHA1281.1